An NMR-based docking model for the physiological transient complex between cytochrome *f* and cytochrome c_6

Irene Díaz-Moreno[a,b], Antonio Díaz-Quintana[a], Marcellus Ubbink[b], Miguel A. De la Rosa[a,*]

[a] *Instituto de Bioquímica Vegetal y Fotosíntesis, Universidad de Sevilla y Consejo Superior de Investigaciones Científicas, Américo Vespucio 49, 41092 Sevilla, Spain*
[b] *Leiden Institute of Chemistry, Leiden University, Gorlaeus Laboratories, P.O. Box 9502, 2300 RA Leiden, The Netherlands*

Received 22 February 2005; revised 11 April 2005; accepted 11 April 2005

Available online 27 April 2005

Edited by Peter Brzezinski

Abstract The physiological transient complex between cytochrome *f* (C*f*) and cytochrome c_6 (Cc_6) from the cyanobacterium *Nostoc* sp. PCC 7119 has been analysed by NMR spectroscopy. The binding constant at low ionic strength is $8 \pm 2\ mM^{-1}$, and the binding site of Cc_6 for C*f* is localized around its exposed haem edge. On the basis of the experimental data, the resulting docking simulations suggest that Cc_6 binds to C*f* in a fashion that is analogous to that of plastocyanin but differs between prokaryotes and eukaryotes.

Keywords: Cytochrome c_6; Cytochrome *f*; Transient interactions

1. Introduction

The electron transfer (ET) between the photosynthetic membrane complexes cytochrome b_6f and photosystem I (PSI) is performed via transient interactions by either cytochrome c_6 (Cc_6) or plastocyanin (Pc). The two soluble redox proteins have different structures, but they share common properties that seem to have undergone parallel variations throughout evolution [1,2]. Thus, the interactions between those proteins and their membrane partners represent an excellent system for comparative studies of transient complex formation. The ET from Pc and Cc_6 to PSI has been extensively studied in a wide variety of organisms, and kinetic data were used to establish a classification of the various reaction mechanisms [1,2]. Kinetic analyses, site-directed mutagenesis [2,3] and structural studies by NMR spectroscopy [4] have led to the identification of the residues of Cc_6 involved in its interaction with PSI. Also, the ET between the soluble domain of cytochrome *f* (C*f*) and Pc has been studied extensively [1], highlighting the role of electrostatic and hydrophobic interactions in binding [1]. NMR studies have enabled the determination of the relative orientations of Pc and C*f* in several Pc–C*f* complexes [5–10]. These studies demonstrate that the position of Pc within the complex is dependent on the extent of electrostatic interactions.

Experimental data concerning the interaction of Cc_6 and C*f* are scarce [1]. A fast-kinetics study using a Zn-Cc_6 derivative has been recently reported [11]. The only structural data correspond to cross-complexes between proteins from different sources [12,13]. Here, we report a study of the interaction between both cytochromes, isolated from the same organism, by chemical-shift perturbation mapping and docking approaches based on ambiguous interface restraints [14]. To our knowledge, this is the first structural analysis of a physiological Cc_6–C*f* complex by NMR spectroscopy.

2. Materials and methods

2.1. Protein preparation

Uniformly ^{15}N-labelled *Nostoc* sp. PCC 7119 Cc_6 was purified as described [10] from *Escherichia coli* cells transformed with both pEAC-WT [15] and pEC86 [16] plasmids. Production and purification of the soluble domain of *Nostoc* sp. PCC 7119 C*f* will be described elsewhere (Albarrán et al., submitted).

2.2. NMR samples

All samples contained 10 mM sodium phosphate, pH 6.0, and 5% D_2O. C*f* was reduced by ascorbate. The binding affinity between Cc_6 and C*f* was estimated by titration of 0.2 mM ^{15}N-labelled Cc_6 with a 3.7 mM C*f* solution. The effect of ionic strength was investigated by adding concentrated NaCl to a C*f*–Cc_6 sample with a [C*f*]/[Cc_6] ratio of 3.

2.3. NMR spectroscopy

2D ^{1}H–^{15}N heteronuclear single-quantum coherence (HSQC) spectra were recorded at 298 K on a Bruker DMX 600 NMR spectrometer. The spectral widths were 26.5 ppm (^{15}N) and 11.5 ppm (^{1}H). Data were processed with AZARA (www.bio.cam.ac.uk/azara), and the resulting spectra were analysed with Ansig for Windows [17]. The spectra were calibrated against the internal standard ^{15}N-acetamide (0.5 mM). Amide assignments of the *Nostoc* Cc_6 were taken from Crowley et al. [12].

2.4. Binding curves

All titration curves were fitted simultaneously to a 1:1 binding model [18] in order to get a single K_A value. Non-linear least-squares fits were performed in Origin 6.0 (Microcal Inc., USA) using the chemical-shift perturbation and the C*f*/Cc_6 ratio as dependent and independent variables, respectively, and the binding constant (K_A) and the maximum chemical-shift change ($\Delta\delta_{max}$) as fitted parameters.

*Corresponding author. Fax: +34 954 460065.
E-mail address: marosa@us.es (M.A. De la Rosa).

Abbreviations: AIRs, ambiguous interaction restraints; Cc_6, cytochrome c_6; C*f*, cytochrome *f*; ET, electron transfer; HADDOCK, high ambiguity driven docking approach; HSQC, heteronuclear single-quantum coherence; Pc, plastocyanin; PSI, photosystem I; RMSD, root mean square deviation

0014-5793/$30.00
doi:10.1016/j.febslet.2005.04.031

Table 1
Active and passive residues, along with flexible segments, used in the definition of the AIRs for docking of Cc_6 and C*f*

Cc_6	
Active residues	S16, A19, L24, A57, K62, G63, R64, K66, E68
Passive residues	K22, K55, N56, P59, P67, E71
Flexible segments	9–9, 16–17, 24–25, 57–65
C*f*	
Active residues	–
Passive residues	Q7, P10, E11, R14, P16, T17, R19, L27, A29, P31, D55, S57, Q59, A63, D64, S66, K67, V68, Y102, Q104, E108, D109, P120, E122, Q123, T163, G164, E165, K166, D190
Flexible segments	1–7, 63–64, 96–97, 102–108, 114–118, 160–163, 188–191

2.5. Chemical-shift mapping

The shifts observed at the last titration point were extrapolated to 100% bound for all residues. The average chemical-shift perturbation ($\Delta\delta_{avg}$) of each amide was defined [19] as $[(\Delta\delta_N/5)^2 + (\Delta\delta_H)^2]^{1/2}$, where $\Delta\delta_N$ and $\Delta\delta_H$ are, respectively, the changes in the ^{15}N and ^{1}H chemical shifts when Cc_6 is 100% bound to C*f*.

2.6. Ambiguous interaction restraints

Ambiguous interaction restraints (AIRs) for the high ambiguity driven docking approach (HADDOCK) docking simulation were generated using standard criteria [14]. Residues labelled as 'active' (Table 1) were those showing $\Delta\delta_{Bind}$ of $^{1}H \geqslant 0.030$ or $^{15}N \geqslant 0.100$ ppm and a solvent accessibility, calculated with NACCESS [20], larger than 50%. For Cc_6, residues at less than 4 Å from the 'active' ones and showing high solvent accessible surface (>50%) were tagged as 'passive'. For C*f*, no 'active' residues were defined and 'passive' residues corresponded to those closer than 15 Å from the haem group and with a high solvent accessibility (>50%).

2.7. Docking protocol

Docking calculations were performed with the HADDOCK suite [14], using homology models of both proteins [3,10] as input. For each run, 2000 rigid-body solutions were generated by energy minimization, using an 8.5 Å non-bonded evaluation cut-off. The 100 structures with lowest AIR restraint energies were subjected to semi-flexible simulated annealing in torsion angle space [14] followed by a final refinement in explicit water [21]. Flexible segments were defined by the 'active' and 'passive' residues used in the AIRs ± 2 sequential amino-acids (Table 1). The non-bonded energies were calculated using the OPLS parameters [22].

2.8. Analysis

The 100 best structures were clustered according to pair-wise root mean square deviation (RMSD) of Cc_6 backbone atoms after aligning backbone atoms of C*f*. RMSD cut-off for clustering was 1.75 Å. Clusters were ranked according to their average interaction energies. The buried surface area was calculated as in [14], using a 1.4 Åprobe radius.

3. Results

To study the interactions between C*f* and Cc_6, a series of ^{15}N–^{1}H HSQC experiments was acquired on a solution of ^{15}N-labelled Cc_6 to which increasing amounts of C*f* were added. A number of Cc_6 amide signals shifted progressively during the titration with C*f* (Fig. 1). Hence, binding and dissociation are fast on the NMR timescale (>100 s^{-1}). A global fit of the data to a 1:1 binding model [18] yields a binding constant of 8 (±2) × 10^3 M^{-1}.

Fig. 2 shows a map of the Cc_6 residues affected by the titration of C*f*. Three stretches of primary structure surrounding the haem cleft are involved in binding to C*f*. Two of them (residues 9–20, except S11, and 23–27) form a hydrophobic patch in which C17 and V25 show the largest chemical-shift changes. The first stretch contains the haem-binding motif CXXCH, including the haem axial ligand H18. The third stretch showing significant $\Delta\delta_{Avg}$ (residues 52–65, except K55 and K62) includes the sixth iron ligand, M58. This residue, along with A60, experiences the largest perturbations of the stretch. No data are available for P59 (marked in grey in Fig. 2). It is noteworthy that E68, at the protein rear, exhibits a medium sized perturbation, like in the cross-complex between *Nostoc* Cc_6 and *Phormidium* C*f* [12].

To study the role of electrostatics in the Cc_6–C*f* complex, the salt effect on chemical-shift perturbations was investigated.

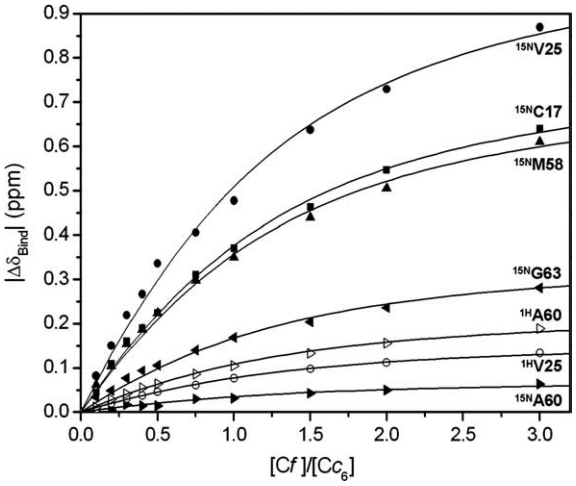

Fig. 1. Binding curves for the physiological interaction between *Nostoc* Cc_6 and C*f*. The absolute value of the chemical-shift perturbation of several amide signals is plotted as a function of the molar ratio of C*f* and Cc_6. Curves represent the best global fit to a 1:1 binding model with K_A = 8 (±2) × 10^3 M^{-1}.

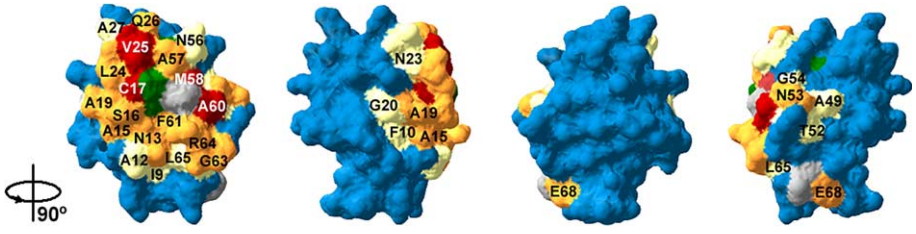

Fig. 2. Chemical-shift perturbation map of Cc_6 in the presence of C*f*. Residues are coloured according to their respective $\Delta\delta_{Avg}$ value (ppm), as follows: blue for <0.025, yellow for ⩽0.050, orange for ⩽0.125, and red for ⩽0.250. Prolines are in dark grey, and the haem group is in green.